The Structure of Hydrous Species in Nominally Anhydrous Minerals: Information from Polarized IR Spectroscopy

Eugen Libowitzky and Anton Beran

Institut für Mineralogie und Kristallographie
Universität Wien - Geozentrum
Althanstraße 14, A-1090 Wien, Austria
eugen.libowitzky@univie.ac.at   anton.beran@univie.ac.at

INTRODUCTION

Hydrogen is a major constituent in a wide variety of minerals in the Earth's crust. Usually H is bonded to oxygen forming H_2O molecules or OH^- groups. In rare cases, H_3O^+, $H_3O_2^-$ and $H_5O_2^+$ units are also formed. The occurrence of NH_4^+, CH_x, etc. in minerals will not be considered here. Hydrogen occurs stoichiometrically in hydrous compounds such as hydrates (e.g., gypsum), (oxy)hydroxides (e.g., goethite), and in many rock-forming silicates (e.g., micas), as well as in nonstoichiometric major amounts in microporous minerals such as zeolites and clay minerals, which are of considerable economic and ecologic importance.

Hydrogen also occurs as a minor or trace constituent in minerals that by definition (and by their formulae) do not contain hydrogen at all, i.e., the so-called nominally anhydrous minerals (NAMs). NAMs include common rock-forming minerals in the Earth's crust (e.g., quartz, feldspars) and upper mantle (e.g., olivine, pyroxene and garnet), but also high-P and high-T phases (e.g., wadsleyite, ringwoodite, and majorite garnet) stable in the mantle transition zone (410-660 km depth).

The aim of the present chapter is to review the use of polarized infrared (IR) spectroscopy as it applies to detecting traces of hydrogen in minerals and to characterizing its speciation and structural environment in nominally anhydrous minerals. The basic theoretical background will be supplemented by a number of examples from recent research. It is important to note that many of the concepts described here for NAMs can also be applied to synthetic compounds of importance in the materials sciences.

The importance of hydrous species in NAMs

Hydrogen may be incorporated as defects in nominally anhydrous minerals of the Earth's mantle. Due to the large volume of rock in the Earth's mantle, even trace concentrations of H in NAMs have the potential to constitute a significant reservoir of H_2O comparable in size to all oceans combined (Beran 1999; Ohtani 2005). Such a large potential water reservoir in the mantle would influence many geologic processes and has several major implications for the evolution of the Earth and atmosphere. Moreover, it is likely that the hydrogen content of the mantle has not been constant over geologic time, but constantly changes in a dynamic water cycle between the hydrosphere and the interior via subduction and volcanism (e.g., Thompson 1992; Dixon et al. 2002; Jacobsen and van der Lee 2006).

Water strongly influences melting temperatures and rheology (e.g., Hirth and Kohlstedt 1996) and thus plutonism, volcanism, and convection. Water penetrates rocks, leaches

elements and leads to the formation of hydrothermal minerals and ore deposits. Release of water and reduced mechanical strength of minerals by dehydration and hydrolytic weakening (Griggs 1967) may even trigger earthquakes in the subducting slab (e.g., Dobson et al. 2002; Jung and Green 2004). Even small amounts of hydrogen, in the form of structural defects, can dramatically change the physical properties of minerals (e.g., Mackwell et al. 1985; Karato 1990). Hydration also influences sound wave velocities and the elastic constants of minerals (e.g., Jacobsen 2006, this volume), which may enable seismologists to detect lateral variations in hydrogen concentrations in the mantle if the effects are large enough and H is present in sufficient quantity (e.g., van der Meijde 2003). In general, incorporation of hydrogen affects the thermodynamic properties of minerals and also influences their kinetic behavior during diffusion (Kohlstedt and Mackwell 1998) and phase transformations (Smyth and Frost 2002). It has to be emphasized that hydrogen-related changes of physical properties are not only interesting with regard to natural processes in the Earth interior, but also for critical parameters in technical applications of crystals (e.g., Buse et al. 1997).

Why use IR spectroscopy?

If hydrogen occurs as a stoichiometric constituent in crystalline solids it can be investigated by diffraction methods (single-crystal X-ray and preferably neutron scattering techniques) and by spectroscopic methods (IR and Raman spectroscopy, proton-NMR spectroscopy). A combination of both techniques provides mutually valuable information on hydrogen in the structure. However, because diffraction depends upon long range order and probes the average structural sites of the major elements in a crystal, it cannot be applied to investigate structural details of non-crystalline materials such as glasses, melts and amorphous minerals, or of trace constituents, such as hydrogen in defect sites of a host crystal. Spectroscopic methods, on the other hand, are highly site specific and do not rely on crystalline periodicity, so they can also be applied to disordered species in liquids and gases. Among vibrational spectroscopic techniques (IR and Raman spectroscopy), IR spectroscopy is ideally suited to investigate even very low concentrations of hydrogen in geologic samples because it is highly sensitive to polar O-H bonds in the structure. When thick samples greater than ~1 mm are used, IR absorption can detect as little as a few wt. ppm H_2O. Moreover, due to the low mass of the H atom, the O-H vibrations and their absorption bands can be easily assigned in the high-energy part of the spectrum between 3000-4000 cm^{-1} and therefore in most cases do not overlap with other peaks from the host lattice.

History

Whereas first simple IR measurements on minerals date back to the beginning of the 20th century, systematic IR investigations of silicate minerals were not made until the 1930s (see Geiger 2004 for a review). However, only in the mid-1950s did IR studies begin to focus on hydrogen in minerals. Early studies were aimed at hydrous minerals such as muscovite (Tsuboi 1950), layered silicates (Serratosa and Bradley 1958), and azurite (Tillmanns and Zemann 1965), which helped to constrain the positions of the hydrogen atoms at a time when it was not possible with X-ray diffraction. Later, IR spectroscopy was also applied to detection of hydrogen in NAMs and confirmed traces of hydrous species in almost every supposedly "dry" mineral (for an earlier review see Rossman 1988). Finally, comparison to well-known structures of stoichiometrically hydrous phases, improvement of quantitative IR data and use of polarized radiation facilitated the development of models for structural incorporation mechanisms. The application and calibration of IR spectroscopy towards analytical water determination was an additional advance in quantitative IR spectroscopy, e.g., Wilkins and Sabine (1973), see also Rossman (2006) in this volume.

CONCEPTS OF INFRARED SPECTROSCOPY

Introduction to IR spectroscopy

Setup of measurements. In a standard IR absorption experiment, a beam of polychromatic IR radiation is emitted from an IR light source, modulated in intensity across the energy (frequency, wavenumber) range by an interferometer and directed through a plane-parallel sample (Fig. 1). Certain energies of light are absorbed by excitation of characteristic vibrations of the material (e.g., by O-H stretching vibrations), and the transmitted light intensity is registered at an IR detector. In modern interferometer-based instruments, the interferogram observed by the detector is mathematically Fourier-transformed to an IR spectrum (thus they are called Fourier transform infrared "FTIR" spectrometers). In an IR absorption experiment, a background spectrum is acquired first (the same setup as above but without sample), recording the incident light intensity at any wavenumber. The sample spectrum is then related to (divided by) this background spectrum giving the transmittance spectrum of the sample. Finally, spectra are usually further converted to an absorbance spectrum (see below).

Basic units and relations. The transmittance (T) is defined by the ratio of the transmitted intensity to the incident intensity (Table 1). T is dimensionless, but conveniently multiplied by 100%. However, a more useful quantity is absorbance (A), which is the negative logarithm of T. Absorbance is linearly proportional to the thickness (t) of the sample and the concentration c of the absorbing species in the sample (see e.g., Libowitzky and Rossman 1996). This relation is expressed by the Beer-Lambert's law: $A = \varepsilon \cdot t \cdot c$, where ε is the molar absorption coefficient. It is obvious (and an advantage of IR absorption spectroscopy) that very low concentrations of an absorbing species can be compensated by using a thicker sample.

The energy scale is conventionally given in wavenumbers (unit: cm^{-1}), because this is proportional to energy and frequency (whereas wavelength is inversely proportional). The frequency of an absorption band equals a vibrational frequency in the sample which is pro-
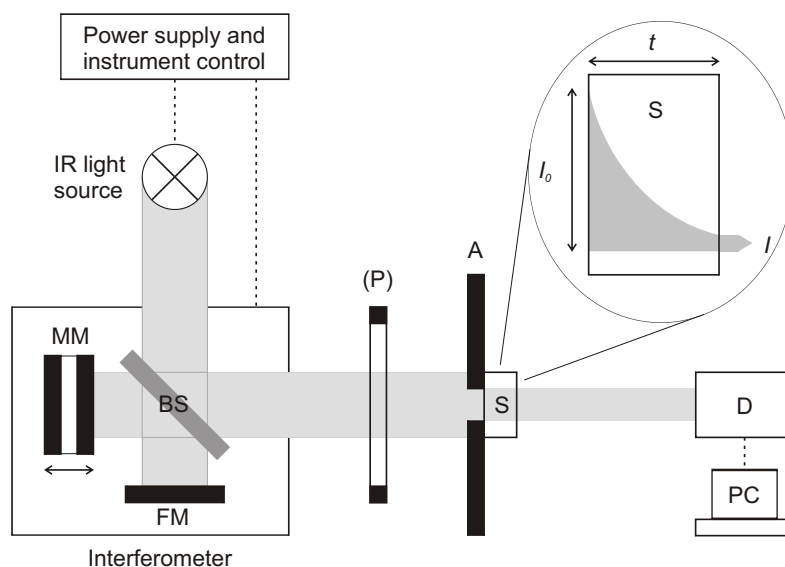

Figure 1. Basic experimental setup of an FTIR spectrometer. A = aperture, BS = beam splitter, D = detector, FM = fixed mirror, MM = moving mirror, (P) = polarizer (optional), S = sample. The close-up shows the exponential decrease of light intensity by absorption with increasing sample thickness.

Table 1. Basic relations and units used in infrared spectroscopy.

$T = I / I_0$	T ... transmittance	A ... absorbance	
$T [\%] = I / I_0 \cdot 100\%$	I_0 ... incident intensity	I ... transmitted intensity	
$A = -\log T$	$T = 10^{-A}$	t ... thickness [cm]	c ... concentration [mol/L]
$A = \varepsilon \cdot t \cdot c$	(Beer-Lambert's law)	ε ... molar absorption coefficient [L cm^{-1} mol^{-1}]	
$A_i = \varepsilon_i \cdot t \cdot c$	(Beer-Lambert's law)	ε_i ... integr. molar absorption coefficient [L cm^{-2} mol^{-1}]	
$A_x = A \cdot \cos^2\alpha$	$A_y = A \cdot \cos^2\beta$	$A_z = A \cdot \cos^2\gamma$	$A_{tot} = A_x + A_y + A_z$
$\nu = \frac{1}{2}\pi\sqrt{f/\mu}$	ν ... frequency [s^{-1}]	f ... force constant	μ ... reduced mass
$\nu = c / \lambda$	c ... speed of light [3.10^{10} cm s^{-1}]		λ ... wavelength [μm]
$E = h \cdot \nu$	E ... energy	h ... Planck's constant	
$\bar{\nu} = 1/\lambda$	$\bar{\nu}$ [cm^{-1}] $= 10^4 / \lambda$ [μm]	$\bar{\nu}$ ... wavenumber [cm^{-1}]	

portional to the square root of the force constant (strength of the chemical bond) divided by the mass of the vibrating atoms (e.g., Libowitzky and Beran 2004). Therefore, the stretching vibrations of H atoms in water and hydroxyl groups (if not or only weakly H bonded) are the highest-energetic fundamental modes in any vibrational spectrum at around 3200-3700 cm^{-1}. However, their band positions are strongly dependent upon the effective strength of the O-H bond which is influenced by the structural environment such as hydrogen bonding and nearest-neighbor cations (see below).

Sample requirements

In order to obtain bulk spectra of minerals, samples are commonly prepared in the form of powder pellets pressed from a mixture of mineral powder heavily diluted in KBr (e.g., 1:200), which acts as an IR-transparent sample medium. Alternatively, the mineral powder is pressed and measured in an ATR (attenuated total reflectance) accessory. However, structural investigations of hydrogen traces in NAMs require oriented, cut and polished slabs of single crystals. These slabs must be free of any impurities such as alterations, inclusions, etc. and ideally be of gem-quality. Because these requirements are almost impossible for large natural samples and many synthetic materials, optically clean areas of available samples are selected by narrowing the beam with a mechanical aperture and/or an IR microscope (see below). Nevertheless, critical evaluation of spectra is necessary to distinguish true structural defects from any kind of extrinsic inclusions (Khisina et al. 2001), especially those that are present at a submicroscopic level.

Experimental equipment

The basic equipment consists of an (FT)IR spectrometer with an energy range of 400-4000 (or even better to 8000) cm^{-1}, a set of apertures with various sizes and an IR polarizer (see below). The given spectral range can be obtained with a single type of light source, beam splitter and detector. However, various alternatives are available which may give higher sensitivity in a more restricted region of the spectrum. Further technical details are given by e.g., Griffiths and de Haseth (1986).

If small samples are investigated (or if small areas of samples have to be selected), a microfocus accessory may be necessary or, even better, an IR microscope. The latter usually facilitates also in-situ investigations under non-ambient temperatures or pressures, using a heating/cooling stage or a diamond anvil cell. Because IR microscopes with conventional black-body light sources are limited to sample areas >20 μm, synchrotron IR radiation was

increasingly used as a light source in the last decade. The extreme brightness facilitates measurements with excellent signal-to-noise ratio down to the diffraction limits <5 μm and detailed mapping of larger sample areas. A review of IR microspectrometry using synchrotron radiation is given by Dumas and Tobin (2003).

QUANTITATIVE DATA FROM INFRARED SPECTROSCOPY

The distance - frequency correlation of hydrogen bonds

If the hydrogen atom of a water or hydroxyl group is attracted by another electronegative atom, usually oxygen or in some cases a halogen, a hydrogen bond is formed. In an O-H···O hydrogen bond, the first oxygen atom is called the donor and the latter the acceptor atom. Though most common in organic molecules and in hydrous compounds, hydrogen bonds are important binding forces in minerals, e.g., between the layers of chlorite-group minerals (Kleppe et al. 2003), and in some cases the only binding force that keeps molecules and coordination polyhedra in a structure together, e.g., in ice (Hall and Wood 1985) and natron (Libowitzky and Giester 2003).

According to the d(O···O) hydrogen bond length, hydrogen bonds are classified as very strong (very short) with d(O···O) < 2.5 Å, strong (short) with $2.5 < d$(O···O) < 2.7 Å, and weak (long) with d(O···O) > 2.7 Å (Emsley et al. 1981). The lower and upper limits are found at 2.4 Å (without external pressure) and beyond 3 Å (with a continuous transition to non-bonded entities). Due to the attractive force of the acceptor, the hydrogen atom is pulled away from the donor and the O-H bond is attenuated compared to a non-bonded unit. Whereas the O-H distance is approximately 0.98 Å in a free hydrous group, it is successively elongated up to 1.20 Å in the shortest hydrogen bonds (which are therefore symmetric without distinction between donor and acceptor atoms). Due to the variability in hydrogen bond distances (and forces) the strength of a hydrogen bond correlates closely with the frequency of its stretching vibration over a wide range of wavenumbers . The common regions are 3200-3750 cm^{-1} for weak H bonds (and non-bonded units), 1600-3200 cm^{-1} for strong H bonds, and 700-1600 cm^{-1} for very strong H bonds.

The bond length vs. stretching frequency correlation of H bonds has been investigated theoretically by Bellamy and Owen (1969), and empirical correlation diagrams have been published since the 1950s, e.g., Nakamoto et al. (1955), Novak (1974), Mikenda (1986), Libowitzky (1999). The diagram for O···O bond lengths in Figure 2 shows the typical positive and curved trend line of the correlation. Scatter of data is caused by deviation of bonds from a straight O-H···O geometry and by influence of cations (see below). In general, it is observed that (very) strong H bonds tend to be more linear, whereas weak ones (such as those mostly observed in hydrous defects) are frequently bent. Further correlation diagrams that may be useful under certain circumstances
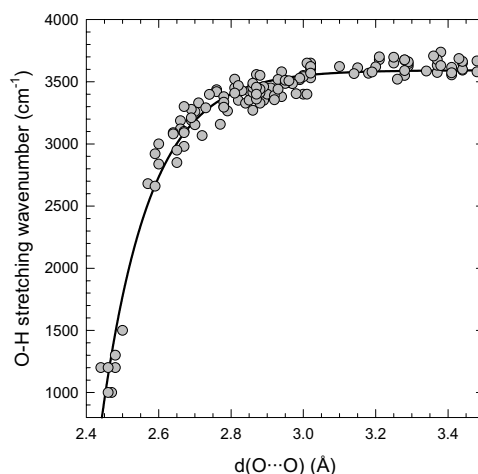

Figure 2. Correlation between hydrogen bond length d(O···O) and O-H stretching frequency (wavenumbers) after Libowitzky (1999).

are stretching frequency vs. $d(H\cdots O)$ by e.g., Libowitzky (1999), stretching vs. $d(O\text{-}H)$ by Novak (1974), stretching vs. bending for OH groups (Novak 1974), hydrogen bond strength vs. $\nu_1\text{-}\nu_3$ splitting of the H_2O molecule (Schiffer et al. 1976). All these empirical correlation diagrams have been obtained by comparison of spectroscopic data with structural data from X-ray and neutron diffraction of hydrous compounds. Thus, in the case of NAMs where only spectroscopic data are available on hydrous defects, they may give important structural information. However, as discussed below, distances obtained from correlation diagrams must be used with caution, because stoichiometric compounds with well-defined hydrogen sites may not be directly comparable with extremely low concentrations of hydrogen atoms located at locally distorted defect sites.

Another correlation with hydrogen bond strength is observed in the band widths of O-H stretching bands. Weak H bonds at high wavenumbers in general reveal sharp bands with small full width at half maximum (FWHM), e.g., a few cm^{-1}. With increasing H bond strength and decreasing wavenumber the band width increases up to several hundred cm^{-1} in case of very strong H bonds (Novak 1974). The reason for this behavior is the increasing anharmonicity of the vibration that correlates also with the increasing H bond strength (Szaly et al. 2002). These extremely broad bands centered at very low wavenumbers that resemble uneven background lines may be recognized in polarized spectra of a few stoichiometric hydrates with high water contents and very strong H bonds (e.g., Hammer et al. 1998), however they have never been observed in NAMs. It may be speculated that they do not exist in the form of defects or that they are simply invisible due to the peculiar background-like shape and the low concentration. In contrast, broad bands in the common O-H stretching region (~2500-3800 cm^{-1}) have been observed in a number of NAMs, e.g., enstatite (Mierdel and Keppler 2004), ringwoodite (Smyth et al. 2003), wadsleyite (Jacobsen et al. 2005), and originate from strong H bonding or other phenomena such as structural disorder. In general, these broad bands and uneven background lines, aggravated by insufficient S/N ratio and small sample size, may affect accurate analysis of water contents in NAMs by IR spectroscopy (see Rossman 2006, this volume).

The spatial orientation of hydrous species

Symmetry considerations. IR radiation traveling through a crystal never affects one individual O-H bond in a single unit cell, but rather many of them at the same time and phase. Thus, the vibrations are not independent and couple in-phase and out-of-phase in various combinations for all symmetry-equivalent entities. The rules for coupling according to symmetry are given by group theory in the form of normal mode analysis for molecules and by factor group analysis for crystals (e.g., Fadini and Schnepel 1989). As an example, the three atoms of a single H_2O molecule in the gas phase (besides 3 translations and rotations in the three coordinates of space) possess three fundamental vibrations: a bending mode (ν_2) above 1600 cm^{-1} and the symmetric and antisymmetric stretching modes (ν_1 and ν_3) with slightly different frequencies above 3600 cm^{-1}. Thus, because of symmetry the vibrations do not occur independently along each O-H vector direction but in a coupled way along the vector sum and vector difference, i.e., parallel and perpendicular to the molecular axis. If more than one H_2O molecule were contained in the primitive unit cell of a stoichiometric hydrate, further combinations of vibrations were possible.

It is an advantage of low concentrations of hydrogen defects in NAMs that the vibrating species are diluted, and coupling of vibrations across many unit cells does not affect the vibrational energies. However, if symmetry-equivalent O-H bonds are grouped together in close vicinity within a unit cell, e.g., in the form of H_2O molecules or clustered OH defects, splitting of bands by symmetry must be considered.

Polarized radiation. In an optically anisotropic (non-cubic) crystal (IR) light is split into two rays with perpendicularly oriented polarization directions vibrating parallel to the main axes of the indicatrix section. In an absorption experiment, light that is already polarized parallel to

one of the indicatrix directions (X, Y, Z) is affected only by the component (A_x, A_y, A_z) of an absorber which is parallel to this polarization direction, i.e., when the electric vector E of the light wave is parallel to (a component of) the oscillating dipole (Fig. 3). This component has a simple cosine squared relationship (Table 1) to the magnitude of total absorbance (Libowitzky and Rossman 1996). Thus, by measuring a crystal section in the two principal polarization directions the orientation of the absorber in this section is obtained. By measuring all three principal polarization directions of the indicatrix ellipsoid, the spatial orientation of the absorber is obtained. Moreover, only the sum of all three polarized component spectra yields the full magnitude of the absorber, i.e., the total absorbance (Libowitzky and Rossman 1996).

Figure 3. Spatial orientation of an absorber A in an orthogonal optical axis system X, Y, Z. Only components of absorption A_x, A_y, A_z can be accessed during an IR absorption experiment with polarized radiation, and facilitate calculation of the spatial orientation of the absorber and the total absorbance (after Libowitzky and Rossman 1996).

Polarizers for IR radiation are available according to two construction principles: (a) wire grid polarizers on an IR transparent material (or even without a support), absorbing radiation parallel to the extremely fine, parallel (gold) wires, polarize radiation over a wide angular range but their efficiency is usually limited to ~1:100. (b) Crystal polarizers, constructed similar to the well-known Nicol's prisms, are made from IR-transparent but strongly birefringent material (e.g., $LiIO_3$). They operate only in a narrow angular range, but their efficiencies may be as high as $1:10^5$.

Total absorbance: a first step towards quantitative water analysis

Due to the logarithmic relation between transmittance and absorbance (see above) only the total absorbance is proportional to the concentration of an absorber. Therefore unpolarized measurements and powder samples of optically anisotropic crystals are not recommended for quantitative measurements. Even the use of low-quality polarizers may bias results (Libowitzky and Rossman 1996). In cases where oriented single-crystals cannot be prepared, statistical analysis of polarized measurements on randomly oriented mineral grains in a rock section can be treated by comparing the measured spectra with polarized reference spectra of the same material (Asimov et al. 2006).

In general, it must be emphasized that only integrated measurement of absorbance (A_i), i.e., the area of a band with properly treated background results in reasonable quantitative data. In that way the various band widths (FWHMs) and even overlapping peaks are reliably evaluated. Correct subtraction of the background line is of high importance. Though a linear background line can be chosen in many cases, problems may be encountered in the case of curved background shape, broad bands (see above) and very low band heights.

Once the total absorbance and thickness of the sample have been measured, the concentration can be calculated according to Beer-Lambert's law. Unfortunately, the molar absorption coefficient is not a unique constant for hydrogen in minerals. In contrast, it varies by orders of magnitude depending upon hydrogen bond strength and stretching wavenumber. Though the linear relation between ε and the wavenumber of the O-H stretching vibration can be used for a general water calibration trend (Libowitzky and Rossman 1997), mineral specific calibrations (in reference to other analytical methods) are preferred. A detailed review of this topic is given by Rossman (2006) in this volume.
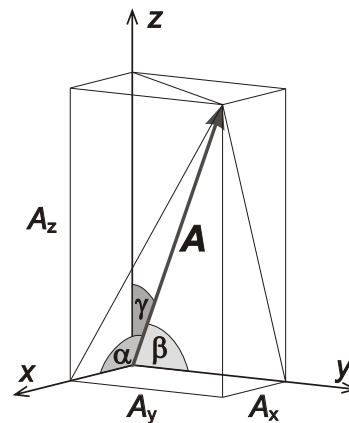
CONCEPTS OF STRUCTURAL MODELS FROM INFRARED DATA

At the beginning of this paragraph it should be stressed that all concepts of structural incorporation models for traces of water in NAMs (whether in the form of H_2O or OH^- defects) have been developed from structural and crystal chemical observations of more or less hydrous minerals, where the information has been extracted from both diffraction and spectroscopy experiments in many cases. Therefore the examples at the end of this chapter contain also hydrous phases with stoichiometric hydrogen.

Charge balance and substitution

Among the principles of crystal chemistry Pauling's five rules (Pauling 1960) represent the most basic ideas on stable ionic compounds. Whereas the first rule comments on bond distances and coordination numbers resulting from the sums and ratios of effective ionic radii, respectively, the second rule comments on charge neutrality. The sum of charges arriving from the ligands at the center of a stable coordination polyhedron equals the (negative) charge of the central atom itself, referred to as the bond strength sum (e.g., Gibbs et al. 2003). In a more general way charge is compensated in the immediate surrounding (coordination sphere) of a charged particle. This principle is also employed in modern structural analysis to check the consistency of a crystal structure and to find hidden hydrogen atoms (missing charges!) in X-ray structural refinements (Brown 1981). This so-called bond valence analysis may even be applied to find preferred oxygen sites for trace hydroxyl substitution in a crystal structure. Thus, the most underbonded O atom in a structure may be considered an ideal docking site for H, e.g., O1 in wadsleyite (Smyth 1987).

Equivalent ideas can be applied to the incorporation of a hydrogen defect in a host crystal structure. If a hydrogen atom (actually a H^+ ion or "proton") enters a crystal structure, its positive charge must be compensated. Or, in other words, if an O^{2-} atom in a crystal structure is replaced by an OH^- group, the missing negative charge must be compensated. An easy way to do so is to change the charge of a neighboring element with different valence states, e.g., $Fe^{3+} + O^{2-} + \frac{1}{2} H_2 \leftrightarrow Fe^{2+} + OH^-$ (e.g., Skogby and Rossman 1989; Koch-Müller et al. 2005). Another common coupled substitution in silicates may involve tetrahedral Si - Al exchange: $Si^{4+} + O^{2-} + \frac{1}{2} H_2 \leftrightarrow Al^{3+} + OH^-$ (e.g., Andrut et al. 2003). Whereas the former process involves only electronic charge transfer, the latter requires exchange of framework atoms and appears more likely to occur during crystal growth than by later diffusion processes. Another substitution mechanism which may easily occur during growth and which does not even require charge compensation is the incorporation of OH^- groups for halogen atoms (F^-, Cl^-) such as in apatite (Baumer et al. 1985) and topaz (see example below). In general, unlike crystal growth the later gain and loss of hydrogen and charge compensating neighbor atoms require diffusion processes which are described in more detail by Ingrin (2006) in this volume.

Probably the simplest way to compensate for the positive charge of an additional H atom is the simultaneous creation of a cation vacancy. This type of defect is known in olivine (Libowitzky and Beran 1995), perovskite (Beran et al. 1996) and others. Even in synthetic high-*P* phases, e.g., wadsleyite (Jacobsen et al. 2005), ringwoodite (Smyth et al. 2003), a clear correlation between H_2O content (up to 1 wt %) and cation vacancies was established. In the hydrogarnet substitution, a cluster of four OH^- groups is facilitated by a Si^{4+} vacancy at a tetrahedral site (see below). The latter has not only been observed as a trace defect but also as a major constituent of natural grossular garnets containing more than 1 wt% of H_2O (Rossman and Aines 1991).

Even if investigation of the correlation mechanisms of hydrogen defects with other substituents by chemical analysis may be an easy task for minerals with considerable H contents and characteristic trace element concentrations, it is almost impossible in cases of hydrogen trace defects (of the order of tens of wt. ppm) because the concentrations of accompanying minor and trace elements in the investigated minerals are commonly higher by orders of magnitude.

Electrostatic considerations on defect geometry

Whereas the electrostatic considerations above provide charge neutrality around a hydrous defect site, the charges of the surrounding atoms also constrain the orientation of an OH^- or H_2O group. Both hydrous species are polar with the negative end at the oxygen and the positive end at the hydrogen atom(s). Therefore, their orientation in a structure is strongly influenced by the attractive and repelling forces of surrounding ions. Because the oxygen atom of an OH^- group is usually part of the crystal structure, it is connected to cations in its first coordination sphere. The same holds true for the H_2O molecule in a number of stoichiometric hydrates.

A characteristic coordination environment around the oxygen atom of a hydroxyl group is a flat trigonal pyramid with the cations at the corners of the base triangle and the OH group on top with the H atom pointing upwards, i.e., perpendicular to the base triangle, away from the other positive charges. This coordination type is an important part of the brucite sheet structure (e.g., Nagai et al. 2000). The orientation of the O-H vector perpendicular to the basal cation plane is caused only by three ions of equal charge, e.g., Mg^{2+}, Mg^{2+}, Fe^{2+}. Substitution of cations by atoms with different valence, e.g., Al^{3+}, Li^+, or even by a vacancy (thus changing also the coordination number) results in considerable deviation of the O-H vector from the normal. A nice example for this type of coordination and the influence of (missing) cations and changed coordination is observed in the mica minerals (Fig. 4). In trioctahedral micas the octahedral layer builds up the regular brucite-type environment of the OH group and thus the O-H vector is aligned exactly perpendicular to the octahedal layer. In dioctahedral micas one third of the octahedral layer cations are missing. Because of this asymmetric distribution of only two positive charges around each OH group, the OH vector is strongly inclined towards the octahedral layer (Beran 2002).

At the proton end, attractive forces of H bond acceptors may influence and distort the orientation of the hydrous defect and lead to elongated O-H bonds resulting in a decrease of O-H stretching frequencies (see above). A contrasting effect (i.e., increase of the stretching wavenumber beyond $3700\,cm^{-1}$) is observed if cations opposite to the proton cause a compressed O-H bond, such as in amphiboles with occupied A site (Rowbotham and Farmer 1973).
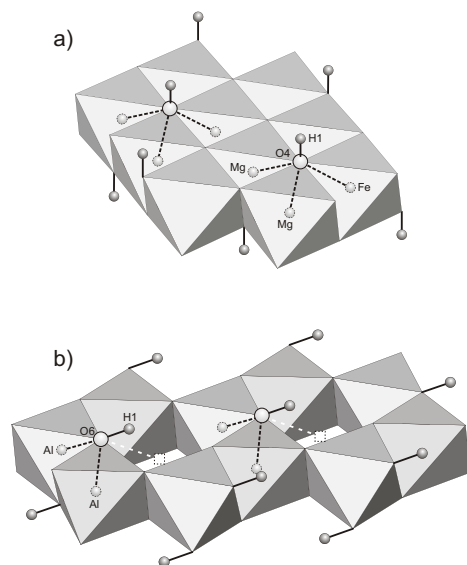

Figure 4. Octahedral layer with OH groups in two mica minerals. (a) Trioctahedral biotite (structural data from Brigatti and Davoli 1990): Three cations (Mg, Fe^{2+}) around the hydroxyl group cause the O-H vector to be approximately perpendicular to the layer (brucite-type coordination). (b) Dioctahedral muscovite (structural data from Rothbauer 1971): The missing third cation (dashed square) in the coordination of the hydroxyl group forces the O-H vector into a tilted direction.

In practice, once the orientation of an O-H vector has been obtained from polarized IR absorption measurements, the probable defect site is considered best by using a three-dimensional ball-and-stick model of the host structure. Thus, electrostatic constraints (see above) can be verified and, moreover, the necessary space (see below) to host a hydrous defect can be investigated. Two-dimensional structure drawings and even animated computer plots may be helpful but they remain always limited in information (as do abstract lists of bond lengths and angles).

Space requirements: ideal and distorted models

Though hydrogen is a very small and mobile ion, the possible arrangements of O-H bonds and of O-H···O hydrogen bonds impose certain space requirements, which are not available at any position in a crystal structure and so help to constrain possible sites of hydrogen incorporation. Data for hydrogen bond lengths derived from stretching vibrations (see above) further help to develop a probable model for a suitable site of hydrogen incorporation. However, as mentioned above in the course of charge balance considerations, the incorporation of hydrous species is charge-compensated by other defects such as different cations or even vacancies in the close neighborhood. Similar to major substitution in solid solution series these structural defects cause distortions of the structure (limiting the use of H bond length calculations) which may be considered in two contrasting ways (e.g., Urusov 1992; Andrut et al. 2004).

VCA model. In the virtual crystal approximation (VCA) model, no structural relaxation around a site of substitution or a defect is assumed and thus the surrounding bond distances represent an arithmetic average of the substituted and unsubstituted geometries, according to the amount of substitution (Vegard's rule). In case of trace defects this would imply an almost unchanged defect environment where calculated H bond distances could be easily applied. Because of the "averaging" and "bulk" character of diffraction methods, their results frequently seem to support the VCA model.

Hard sphere model. In the hard sphere model, full relaxation of the structure around a "hard" substituent or defect is assumed. Thus the defect environment, e.g., bond distances, develops undisturbed, as if the whole structure would consist to 100% of this substitution or defect. Because of the two different environments (with and without defect/substitution) at a single site, spectroscopic methods are superior to reveal the real situation in the structure.

The real situation, expressed by the degree of relaxation (Urusov 1992), is usually found between these two extremes. The example of the hydrogarnet substitution (see below) elucidates the power of IR spectroscopy to identify the true defect environment and points out the limits of theoretical H bond calculations.

Influence on band energies from cation substitution

Substitution of cations by elements with different valences and even by vacancies in the vicinity of hydrous defects has been discussed above as an important mechanism to achieve charge neutrality. Another aspect of cationic substitution is that different cations in the neighborhood and coordination sphere of, for example an OH⁻ group may affect the energy of the O-H stretching vibration by more than 50 cm^{-1}. In turn, shifts and splitting of absorption bands may indicate different cationic surroundings of OH defects in crystal structures.

Substitution of Mg by different cations (e.g., Mn, Zn, Ni, Fe^{2+}, Fe^{3+}) and formation of solid solution series in common silicates with the brucite-type OH coordination such as amphiboles and talc shows interesting results. The band shift to lower wavenumbers is linearly correlated with increasing electronegativity of the substituting element, i.e., from Mg to Fe^{2+} and further to Fe^{3+} (Strens 1974). Moreover, even the number of substituents can be derived from the spectra. An intermediate Mg-Fe actinolite shows four equally spaced OH stretching bands (Fig. 5), which can be correlated according to their intensities and by comparison to pure endmember tremolite to four cationic environments around the OH group (Burns and Strens 1966): MgMgMg (~3670 cm^{-1}), MgMgFe, MgFeFe, FeFeFe (~3625 cm^{-1}).
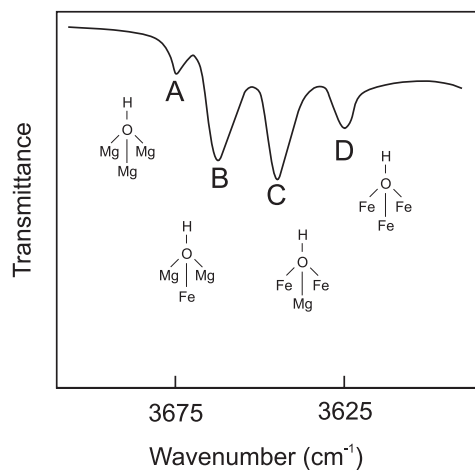
Figure 5. The four O-H stretching bands in an intermediate Mg-Fe-actinolite and their assignment to different cationic environments. Modified after Burns and Strens (1966).

Discrimination among hydrous defects

Single OH$^-$ group. A single hydroxyl group, i.e., a trace defect without any symmetry-equivalence in its close vicinity, is characterized by a single band whose position is mainly dependent upon the strength of hydrogen bonding (see above). Nevertheless, it is commonly observed in the 3000-3750 cm^{-1} region. However, because this single defect may occur with different cationic environments in different parts of the crystal (e.g., MgMgMg or MgFeMg, see above) every type of environment and even a vacant site may cause a separate band. Further vibrations which are caused by an OH$^-$ group are a Me-O-H bending mode around 700-1400 cm^{-1} (depending also upon H bond strength) and the combination mode of the stretching and bending vibrations around 4500 cm^{-1}. However, if a hydroxyl defect occurs only in trace concentration, the former is usually hidden by the strong vibrations of the host mineral, and the latter may be too weak to be detected.

Single H$_2$O molecule. Because of its symmetry an undistorted water molecule possesses two stretching vibrations, one symmetric and one antisymmetric mode. As for all O-H vibrations their band positions depend upon H bonding, but are frequently observed in the 3000-3750 cm^{-1} region, meaning that they cannot be distinguished from bands of OH$^-$ groups. Fortunately, the water molecule also has a bending mode at approximately 1600-1650 cm^{-1}, which is a characteristic feature of this unit. Another characteristic band may be observed at ~5200 cm^{-1}, which is the combination of stretching and bending vibrations. However, because of its weak intensity it may be invisible at trace concentrations.

H$_3$O$^+$ group. Hydronium (if present as the only hydrous species) is identified by four vibrations with a characteristic bending mode around 1100 cm^{-1} (Nakamoto 1977). All these vibrations are similar to water and hydroxyl stretching and bending modes, so that they cannot be distinguished unambiguously from a combination of different H$_2$O or H$_2$O + OH$^-$ species.

H$_3$O$_2^-$ group. This unit, which has been considered to possess a symmetric, very short hydrogen bond in its center, has only been observed in stoichiometric phases (e.g., Beran et al. 1997). These investigations confirmed the (very) strong central hydrogen bond, but indicated also the non-symmetric configuration of the bond. Thus, the unit is considered as a linked H$_2$O plus OH$^-$ group. The observed vibrations are the stretching modes of the terminal O-H units at high wavenumbers, the stretching mode of the central (very) strong H bond at low wavenumbers, and the bending mode of an H$_2$O unit. Because of the very broad band shape of

the (very) strong central H bond (see above) it is unlikely that this feature is found at minor or trace concentration levels.

H₂ molecule. Due to its high symmetry the H_2 molecule is only Raman active with a stretching vibration at ca. 4155 cm^{-1}. Though observed by micro-Raman spectroscopy in special fluid inclusions in melts and glasses (if present as a major constituent), it is unlikely to occur commonly as a structural defect in minerals. Nevertheless, it should be stressed that, except under very peculiar circumstances (distortion of the molecular symmetry by attraction of H_2 to the host structure), IR spectroscopy is not suited to detect H_2 in minerals.

Clusters of hydrous defects. Clusters of vibrating O-H units (in principle, an H_2O molecule is a simple cluster of two O-H vectors with a common O atom) are identified by more than one vibration according to their symmetry (see above). Unfortunately, this is not an absolute necessity, as is demonstrated in the case of $(OH^-)_4$ clusters in hydrogarnet (see below), which are characterized by a single OH stretching band (Rossman and Aines 1991). However, charge balance considerations (in this case a vacancy at the Si^{4+} position) indicate the necessity of more than one OH^- group.

Hydrous inclusions. One of the pitfalls of IR spectroscopic identification of hydrous defects is that even microscopically clear, gem-quality samples may include sub-microscopic fluid inclusions that resemble true structural defects. Fluid inclusions are readily identified by their characteristic broad water bands around 3400 cm^{-1} and by the appearance of sharp ice bands upon freezing. However, inclusions of hydrous minerals may be very difficult to identify. This problem has been discussed by Khisina et al. (2001). In other cases, however, IR spectroscopy may be the perfect tool to identify "invisible" mineral inclusions by their characteristic fingerprints in the OH stretching region, e.g., kaolinite in kyanite (Wieczorek et al. 2004) or corundum (Beran and Rossman 2006). During heating (either by nature or by experiment) these hydrous inclusions may act as a source of hydrogen to incorporate further structural defects.

Deuteration

Though the fingerprint of O-H stretching vibrations can usually be distinguished from the fundamentals and overtones of the host mineral, problematic cases need additional treatment. Because diffusion of hydrogen at elevated temperatures is rapid, the isotope deuterium (D) can be incorporated into the material in exchange for hydrogen (Ryskin 1974). Due to the dependence of vibrational frequencies on mass (see above), corresponding O-D bands are observed at lower wavenumbers, shifted by a factor of ~1.35 (depending upon H bonding and anharmonicity, the latter also causing deviation from the ideal value $\sqrt{2}$).

The reduced anharmonicity of O-D stretching vibrations in comparison to O-H modes may also result in sharper peak shapes helping to deconvolute interfering absorption bands. The problem of overlapping bands may also be solved by cooling samples to liquid nitrogen temperature in a cooling stage (see above), which may lead both to reduced FWHM and variable shifts of the peaks.

EXAMPLES

Vesuvianite: orientation and hydrogen bonding of hydroxyl groups

Vesuvianite, ~$Ca_{19}(Mg,Fe)_3(Al,Fe)_{10}Si_{18}O_{70}(OH,F)_8$, is an ideal first example to demonstrate the power of quantitative IR data using the wavenumber vs. hydrogen bond distance correlation and polarized spectra to constrain the O-H vector orientations. Though a chemically complicated sorosilicate (Groat et al. 1992), two different hydroxyl groups can be clearly distinguished in the structure, which have also been determined by neutron diffraction (Lager et al. 1999). The latter is the reason for the selection of a hydrous mineral as example rather than a NAM.

Figure 6 shows polarized IR absorption spectra of a (*hk*0) slab of tetragonal vesuvianite with the **E** vector of light vibrating parallel and perpendicular to the *c* axis, respectively. Bands of the **E**//*c* spectrum are obviously more intense than those of the **E**⊥*c* direction. There is a strong band around 3100-3200 cm⁻¹ and a group of strong bands between 3450 and 3700 cm⁻¹. The former is quite broad and its low wavenumber indicates a hydrogen bond distance of *d*(O···O) ~ 2.70 Å (Libowitzky 1999). Its intensity perpendicular to *c* is zero and thus indicates an O-H orientation parallel to the *c* axis. The latter bands are sharper and their wavenumbers indicate only weak or no hydrogen bonding. Exact evaluation of the band areas in both polarization directions confirms an O-H vector orientation of ~35° tilted from the *c* axis (Bellatreccia et al. 2005). The identical pleochroic behavior of all high-energy bands indicates one hydroxyl site with different cationic environment resulting in the slightly different positions of these bands.

The inset of Figure 6 shows a detail of the vesuvianite structure and confirms the band assignment from above. There is actually a moderately strong hydrogen bond at H(2) with *d*(O10···O10) ~ 2.72 Å (Lager et al. 1999), the O(10)-H(2) vector pointing exactly parallel to the *c* axis. Another hydroxyl group is located at O(11)-H(1) confirming the acute angle towards the *c* axis and various cations in its environment. Its weak, bifurcated H bond is in good agreement with the high wavenumbers of the IR bands.

Quantitative measurements of the OH content in vesuvianites by IR spectroscopy and SIMS analyses (Bellatreccia et al. 2005) confirmed the general calibration trend of Libowitzky and Rossman (1997), although it had been demonstrated to be inaccurate for a number of NAMs.

Hydrogarnet substitution - the (OH)₄⁴⁻ cluster

Garnets contain a wide range of water concentrations, starting from a few wt. ppm in mantle garnets up to several wt% in samples of the grandite (grossular-andradite) series (Beran and Libowitzky 2006). However, their optically isotropic character, their complicated chemistry
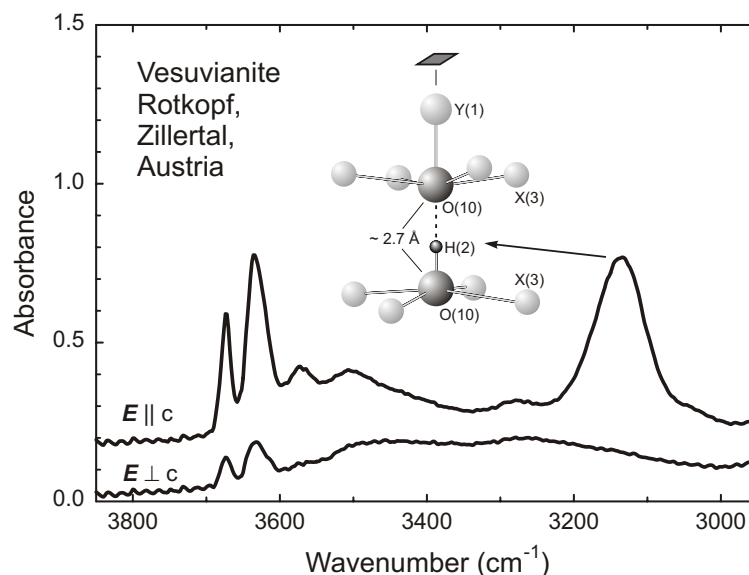
Figure 6. Polarized IR absorption spectra of vesuvianite (data from Kurka 2002). The strong band at ~3100 cm⁻¹ occurs only in the *c* spectrum and indicates by its low wavenumber a moderately strong hydrogen bond, which is readily assigned to O(10)-H(2)···O(10) in the structure of vesuvianite (modified after Lager et al. 1999).

due to a number of solid solution series, and a wide variety of observed OH stretching modes at rather high wavenumbers (3500-3700 cm^{-1}) (indicating absence of hydrogen bonding) makes unambiguous identification of distinct OH$^-$ defects in silicate garnets difficult.

In contrast, the high concentration of water in certain grossular garnets facilitated investigation by diffraction, analytical and spectroscopic methods, which revealed four OH$^-$ groups substituting for a SiO$_4^{4-}$ group, i.e., the (OH)$_4^{4-}$ cluster in the so-called hydrogarnet (hydrogrossular) substitution. Figure 7 shows the configuration of this cluster in comparison with a common silicate tetrahedron. With regard to the theoretical considerations on defects in crystal structures above, a number of interesting features are observed.

The incorporation of four protons is charge-compensated by a Si^{4+} vacancy. Thus, charge balance is achieved in the closest vicinity (coordination sphere) of the defect site. However, the four hydrogen atoms are not

Figure 7. A silicate tetrahedron (left) and the hydrogarnet substitution (right) indicating the increased size of the tetrahedron, the empty Si^{4+} position (square) and the H atoms above the tetrahedral faces (structural data from Lager et al. 1987).

placed inside the tetrahedron (pointing towards the empty silicon site) as was proposed in an earlier paper (Sacerdoti and Passaglia 1985). Although this configuration might be considered an ideal mechanism for local charge compensation for the missing Si^{4+}, it is not favorable due to electrostatic repulsion of the four protons in close proximity to each other. More recent papers confirm that the positions of the H atoms are, instead, rather slightly above (outside) the faces of the tetrahedron (e.g., Lager et al. 1987).

Because of the missing central charge of Si^{4+}, the size of the hydrogarnet tetrahedron is increased by ~20 % with respect to the silicate tetrahedron (Si-O ~ 1.65 Å, □-O ~ 1.95 Å) in pure endmember hydrogrossular. The corresponding IR spectrum shows a single absorption band at 3660 cm^{-1} (Rossman and Aines 1991). This high wavenumber is in agreement with only weak or no hydrogen bonding along the edge of the tetrahedron (O···O > 3 Å). Intermediate solid solutions that contain both silicate and hydrogrossular tetrahedra are characterized by two bands at 3600 and 3660 cm^{-1} with different intensities. This classical two-mode behavior was interpreted by a pure hydrogrossular environment (band at 3660 cm^{-1}) and an (OH)$_4^{4-}$ defect surrounded by silicate tetrahedra (3600 cm^{-1}). The latter wavenumber is still in agreement with only weak hydrogen bonding in a strongly inflated tetrahedron and thus confirms the hard sphere model. If, in contrast, the VCA model (see above) were pertinent, wavenumbers at low hydrogarnet concentrations would be expected at rather low wavenumbers due to short O···O distances in a □$_{Si}$O$_4^{4-}$ tetrahedron with almost unchanged size.

Finally, it should be emphasized that the hydrogarnet substitution is not limited to grossular garnets, but has also been observed at low concentration levels in pyrope (Beran et al. 1993; Geiger et al. 2000) and even other minerals outside the garnet group, e.g., hydrozircon (Caruba et al. 1985). Moreover, the replacement of Si^{4+} by a cluster of four protons has been proposed as an important hydrogen incorporation mechanism by atomistic simulations (see also Wright 2006, this volume) for e.g., olivine (Braithwaite et al. 2003) and ringwoodite (Blanchard et al. 2005). With Ti^{4+} substituting for Al^{3+} in close vicinity to the tetrahedral (vacant) site, even an incomplete cluster of [(OH)$_3$O]$^{5-}$ was suggested in pyrope by Khomenko et al. (1994). The combination of the hydrogarnet cluster with moderately strong hydrogen bonding was observed in the tetragonal garnet henritermierite (Armbruster et al 2001), where the distorted octahedron around Mn^{3+} provides an oxygen atom acting as H bond acceptor at rather close distance. In a
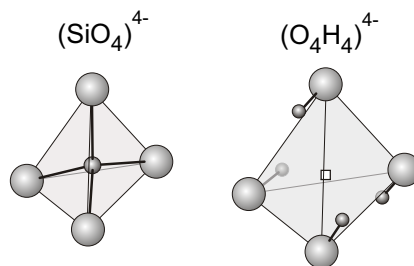
suite of non-cubic garnets of the grossular-uvarovite join, Andrut et al. (2002) observed a number of varieties of the hydrogrossular substitution related to pleochroic IR absorption bands.

Water molecules in structural cavities: beryl and cordierite

The framework silicates beryl, $Be_3Al_2Si_6O_{18}$, and cordierite, $Mg_2Al_4Si_5O_{18}$, contain structural units of 6-membered rings of tetrahedra which are stacked in such a way that channels parallel to the hexagonal *c* axis (in beryl) and parallel to the two-fold *c* axis (in orthorhombic low-cordierite) are formed. Both sets of channels are lined with oxygen atoms from the tetrahedral ligands, and with a maximum width of ~5.1 Å, separated by bottlenecks of ~2.8 Å, they can be occupied by alkalis, H_2O and CO_2 molecules (Kolesov and Geiger 2000a,b).

Vibrational spectra contain water stretching and bending modes with wavenumbers around 3550-3700 cm^{-1} for stretching vibrations (Aurisicchio et al. 1994) indicative of weak or no hydrogen bonding. This is consistent with water molecules contained in the wide cavities of the channels (Fig. 8). The pleochroism of H_2O stretching and bending vibrations in Raman and IR spectroscopic experiments confirms two possible orientations of the H_2O molecule: Type I is oriented with the molecular axis perpendicular to the channel axis, whereas type II is oriented parallel to *c*. It is interesting to note that, although both stretching vibrations of H_2O (ν_1 symmetric, ν_3 antisymmetric stretching) are IR and Raman active, due to strongly different activation cross sections, only ν_3 occurs at 3700 cm^{-1} in IR spectra with **E** parallel to *c* for type I H_2O, whereas Raman spectra yield only ν_1 at 3607 cm^{-1} (Kolesov and Geiger (2000a). Type I H_2O is predominantly observed, if alkalis are absent from the channels of the structure, whereas type II is found together with alkali ions (Aurisicchio et al. 1994). Considering the polar character of the water molecule, the structural incorporation model according to Figure 8 was developed. Moreover, as suspected from IR spectra, another possible type of incorporation in the form of an OH^- group attached to a large alkali ion can be derived.

Studies at variable temperature showed that type I water is dynamic and "rotates" about the channel axis down to very low temperatures (Winkler 1996). A recent study by Gatta et al. (2006) shows that this "rotation" is better described by a dynamic disorder of the water molecule over 6 equivalent positions. With increasing temperature both types of water approach the gaseous state followed by dehydration without destruction of the mineral structure (Aines and Rossman 1984).
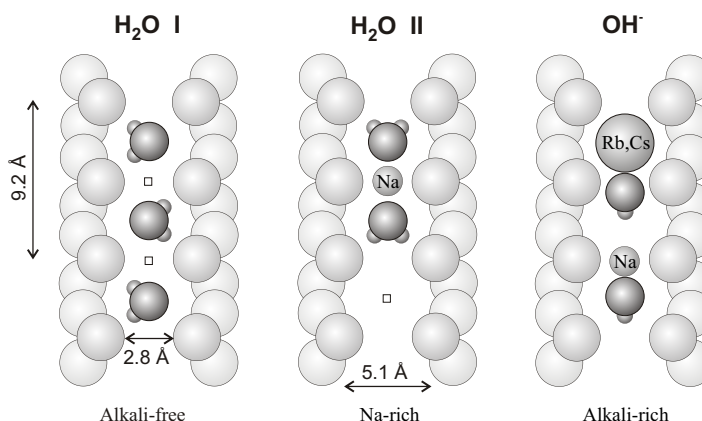

Figure 8. Three types of hydrous species in the structural channels of beryl (and similarly of cordierite). H_2O I occurs preferably in alkali-free channels, H_2O II in alkali (Na)-rich channels, and OH^- ions are considered in correlation with large alkalis (Rb, Cs). Modified after Aurisicchio et al. (1994).

OH substitution in topaz

Although topaz has been studied by IR and Raman spectroscopy in a number of investigations (Gebert and Zemann 1965; Aines and Rossman 1985; Beny and Piriou 1987; Wunder et al. 1999; Bradbury and Williams 2003), all these papers lack one or another aspect of spectral evaluation. Therefore, we decided to demonstrate a worked example on a new topaz data set that has not been published previously. Moreover, we chose topaz because it contains a single OH group (with a single IR absorption band) substituting for the fluorine atom in its structure and because its orthorhombic symmetry is ideal for geometric considerations.

A clear, colorless, gem-quality topaz crystal from Spitzkoppe, Namibia with a size of $9 \times 11 \times 17$ mm was chosen for this study. The F-rich composition of this specimen, $Al_2SiO_4F_{1.85}(OH)_{0.15}$, $(OH)/(OH + F) = 0.075$, was confirmed by the correlation of Ribbe and Rosenberg (1971) using the lattice parameters from X-ray powder diffraction (space group *Pbnm*, $Z = 4$, $a = 4.652$ Å, $b = 8.804$ Å, $c = 8.390$ Å, CuKα, 5% Si standard). The sample was oriented according to the excellent cleavage parallel to (001) and along the optical extinction directions (optical setting: $a = X$, $b = Y$, $c = Z$). Three platelets (100), (010), (001) were cut from the sample, attached with crystal bond epoxy resin to a glass plate sample holder and diamond-polished to a final thickness of ~15 μm (uncertainty due to resin layer). To retain the large size of the extremely thin sections they were not removed from the glass plate, and spectra were corrected for background absorption from glass and epoxy resin.

Figure 9 shows the polarized spectra of topaz in the O-H stretching region parallel to the three main axis directions with a strong absorption band at 3649 cm^{-1} and Figure 10 gives the angular absorption plots of the integrated absorbance of the OH stretching band in all three crystal sections. Both figures confirm that the absorption is almost zero parallel to the *b* axis (*Y*) direction. Thus the O-H dipole must be aligned within the (010) plane. Further inspection of the (010) angular absorbance plot (Fig. 10) and comparison of the *X* and *Z* directions (Fig. 9) indicate a preferred O-H orientation along the *c* axis (*Z*) direction. The ratio of the *Z:X* integrated band intensities is ~2:1, and application of the cosine squared relation (Table 1) results in an angle of ~35° between the O-H dipole and the *c* axis direction.

This result is in excellent agreement with diffraction data (Zemann et al. 1979; Parise et al. 1980; Belokoneva et al. 1993) that yield ~29°, and also with crystal chemical considerations. Figure 11 shows the environment of the OH group in the structure of topaz. The repelling forces of the two Al atoms coordinating the OH group are such that the H atom is aligned almost exactly within the Al-O-Al plane and bisects the Al-O-Al angle. The weak H bonds around the H atom are in agreement with the high wavenumber position of the OH absorption band and have only a very minor influence on the alignment of the O-H vector.

Finally it should be emphasized that the OH stretching band of F-rich topaz is not a single band but rather contains another component at ~3640-3646 cm^{-1} (depending upon peak fit constraints). This feature has been frequently ignored in older literature on topaz with low H content, but it was definitely described and discussed in recent papers on synthetic OH-rich topaz, e.g., Wunder et al. (1999). These details of peak fitting will be presented and discussed in a separate paper (Libowitzky, in prep.).

OH incorporation in diopside

Pyroxenes contain significant amounts of hydrogen with concentrations ranging from a few 10s to more than 1000 wt. ppm H_2O. Thus, pyroxene may indeed be a major storage site for hydrogen in the Earth's upper mantle (Skogby 2006, this volume, and references therein).

IR spectra of clinopyroxenes (cpx), i.e., diopside-hedenbergite, augite, and omphacite, are characterized by four regions of pleochroic OH stretching bands centered at 3630-3640, 3530-3540, 3450-3470 and 3350-3360 cm^{-1} (the latter only in a number of diopsides). Two different
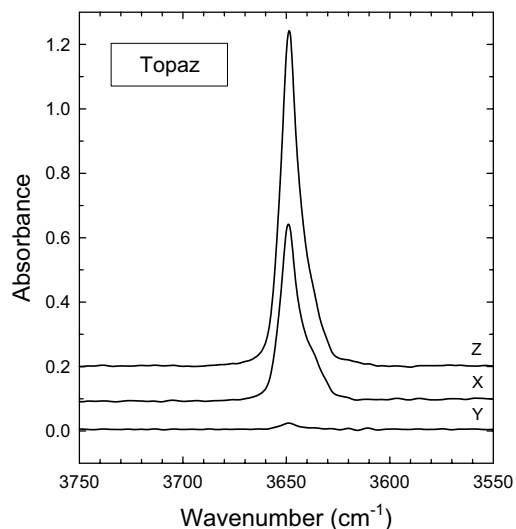
Figure 9 (*left*). Polarized IR absorption spectra of colorless topaz from Spitzkoppe, Namibia, in the O-H stretching region parallel to the three principal axis directions. Sample thickness: ~15 μm, Perkin Elmer 1760X FTIR spectrometer (ceramic light source, KBr beam splitter, TGS detector), gold wire grid polarizer (efficiency ~ 1:100), circular sample aperture: 4 mm diameter, spectral resolution: 4 cm^{-1}, 32 scans each averaged.
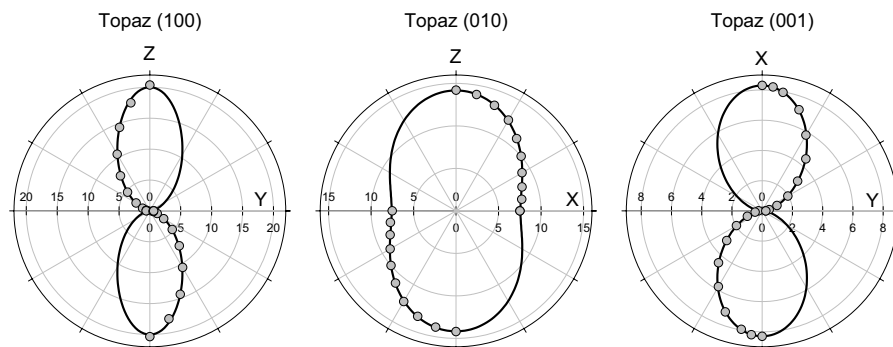

Figure 10 (*above*). Absorbance figures depicting the pleochroic scheme of the O-H stretching band of topaz (integrated absorbance vs. sample to polarizer angle). Lack of absorbance parallel to the *b* axis (*Y*) indicates an O-H vector orientation in the (010) plane. The anisotropic absorbance in (010) indicates an O-H orientation closer to the *c* axis (*Z* direction).
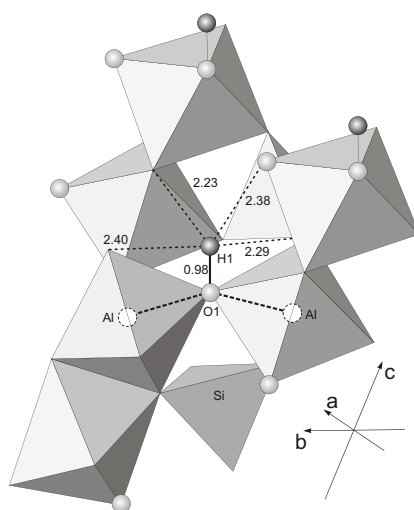

Figure 11 (*left*). The environment of the hydroxyl group in the structure of topaz. The view was chosen in such a way that the OH group in the center of the picture and the two coordinating Al atoms (broken circles, connected by bold broken lines) are in the plane of projection. Broken lines indicate weak H···O bonds, the numbers give distances in Å. Structural data from Zemann et al. (1979).

types of pleochroic behavior can be distinguished. Bands in the 3630-3640 cm^{-1} region are α- and β-polarized (group I bands), the lower energetic bands are γ-polarized (group II bands). Compare to Figure 12 in this chapter, and Table 1 in Skogby (2006), this volume. The two types of pleochroic bands suggest that at least two types of OH positions exist simultaneously in the diopside structure (Beran 1976; Ingrin et al. 1989; Skogby and Rossman 1989; Skogby et al. 1990). The position and pleochroism of the absorption bands are similar for different cpx samples, but the absolute intensities vary strongly, e.g., spectra of omphacites with jadeite-rich compositions show a strong γ-polarized absorption band at 3460-3470 cm^{-1}, whereas those with diopside-rich compositions reveal a strong α-polarized band at 3620 cm^{-1} (Smyth et al. 1991). As an example for OH defect characterization by polarized IR spectroscopy, the study of a hydrothermally formed, gem-quality diopside crystal from Rotkopf, Tyrol, Austria, is given below (Andrut et al. 2003).

The extremely strong pleochroism of the high-energy group I band in (010) sections at 3647 cm^{-1} (Fig. 12) suggests a strong preferred orientation of the OH dipole approximately parallel to the α index of refraction, i.e., the direction of the long diagonal of the unit cell projection parallel to [010] (Fig. 13). The moderate pleochroism of this band in (100) with a stronger component parallel to [010] (equivalent to n_β) indicates a strong deviation of the OH vector direction from an alignment within the (010) plane. These results confirm the model proposed by Beran (1976) that OH defects partially replace the O2 "zigzag" oxygen atoms pointing to the O3 oxygen atom of a neighboring silicate chain (Fig. 13). O2 is coordinated by 1 Mg, 1 Ca and 1 Si, thus forming the top of a flat slightly distorted trigonal pyramid, being an ideal candidate for a partial OH replacement. This replacement mode also occurs in a 1100 °C temperature-treated crystal and evidently represents a very stable OH defect position. Another model of OH defect incorporation on O2 sites (with similar O-H vector orientation) can also be derived under the assumption of a vacant *M*1 site, resulting in a coordination of the OH defect by Ca and Si.

Owing to the pleochroism of the low-energy band doublet at 3464 and 3359 cm^{-1} in (010) (Fig. 12), the OH dipole direction must be oriented roughly parallel to the γ index of refraction, i.e., the direction of the short diagonal in the (010) section of the unit cell. In addition, a slight deviation from the (010) plane is indicated. An OH dipole direction that is in agreement with the observed pleochroic behavior can be provided under the assumption of *M*2 vacancies. OH defects coordinated by 1 Mg and 1 Si are generated by a partial replacement of O2 oxygen atoms with an orientation pointing strongly above the Ca vacancy site. The separation of the low-energy bands is explained by a replacement of the coordinating Mg by Fe or Si by Al.
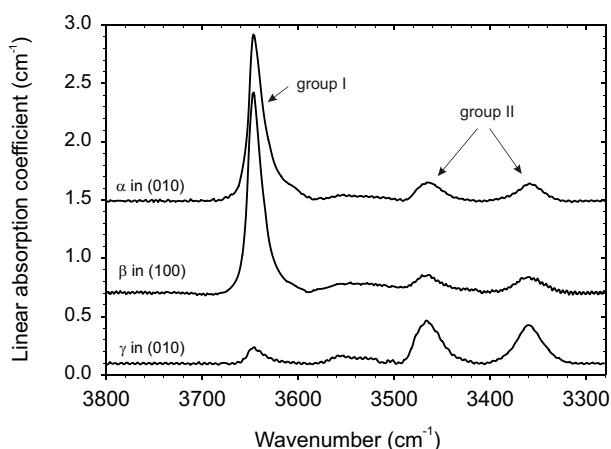

Figure 12. Polarized OH absorption spectra of light-green diopside from Rotkopf, Zillertal, Tyrol, Austria, measured on (100) and (010) plates (modified after Andrut et al. 2003).

OH defects in perovskite

(Mg,Fe)SiO$_3$ perovskite is most likely the major mineral phase in the Earth's lower mantle and its role as a storage site for hydrogen has been recently discussed in review articles by Bolfan-Casanova (2005) and Ohtani (2005). On the other hand, though being a rare mineral, natural CaTiO$_3$ perovskite forms in various geological environments, including kimberlitic rocks, and shows a wide range of compositions (Hu et al. 1992). Based on Paterson's (1982) calibration, Beran et al. (1996) reported about 70 wt ppm H$_2$O in perovskite of metasomatic origin.

The IR spectrum of OH containing CaTiO$_3$ perovskite consists of two bands with maxima centered at 3394 and 3326 cm^{-1} (Fig. 14). From the weak pleochroism of the bands in (001) and the more distinct pleochroism in (110), with a stronger component of absorption perpendicular to [001], an OH direction roughly pointing along [110] with the O2 oxygen atoms acting as donor is deduced (inset of Fig. 14). Using the hydrogen bond length vs. stretching frequency correlation of Libowitzky (1999), excellent agreement between the expected (calculated) H bond lengths and the actual O···O distances in the structure (2.75-2.78 Å) is obtained. The O-H vector orientation is facilitated only by the presence of a vacant Ca site (Beran et al. 1996, inset of Fig. 14). The OH defect positions coordinated by two Ti and one Ca atoms correspond to those proposed by Meade et al. (1994) in synthetic high-pressure MgSiO$_3$ perovskite, where OH bands occur at 3483 and 3423 cm^{-1}. Similar to CaTiO$_3$ perovskite, the assumption of a vacant Mg position seems necessary from geometric and electrostatic considerations.

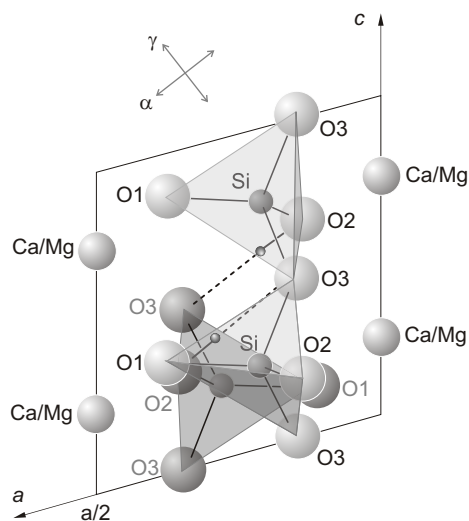In contrast, high-*P*,*T* experiments performed by Bolfan-Casanova et al.

Figure 13. Part of the diopside structure projected parallel to [010] with OH defects at O2 pointing to O3 of a neighboring silicate chain (modified after Beran 1999). Dark grey atoms, labels and tetrahedron belong to the silicate chain behind the light grey units.
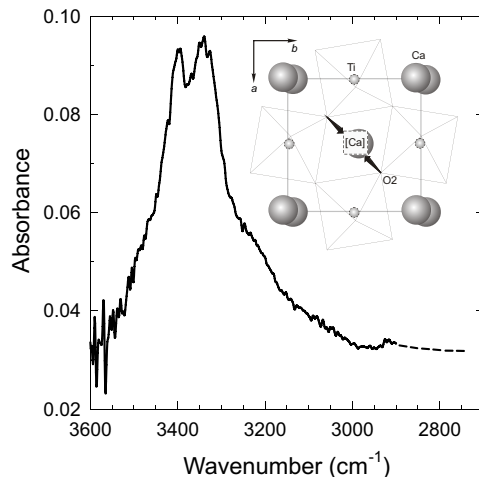

Figure 14. IR absorption spectra of perovskite. The inset shows the structure of perovskite. The two arrows, deviating from the plane of projection, indicate possible O-H vectors close to a vacant Ca site (modified after Beran et al. 1996).

(2000) in the MgO-SiO$_2$-H$_2$O system did not detect any OH in MgSiO$_3$ perovskite. Whereas MgSiO$_3$ akimotoite, coexisting with MgSiO$_3$ perovskite, synthesized at 24 GPa and 1600°C dissolved significant amounts of water (see below), perovskite was essentially dry.

The conflicting experimental findings of Bolfan-Casanova et al. (2000) and Meade et al. (1994) might be related to the different synthesis conditions of the two studies. In the former study the sample was held at P and T for 3.5 hours, in the latter study for only several minutes. Therefore, any defects in $MgSiO_3$ perovskite may have been annealed out in the Bolfan-Casanova et al. (2000) study whereas they were retained in the latter. Therefore, the presence of vacancies at the Mg site (see above) may be a key factor whether $MgSiO_3$ perovskite incorporates OH groups in its crystal structure or not (Ross et al. 2003). Moreover, under natural conditions, the lower mantle contains elements, such as Fe and Al, which have not been involved in the synthesis and which may facilitate OH incorporation in perovskite (Bolfan-Casanova 2005).

OH traces in corundum

The presence of OH in corundum as accessory mineral of mantle rocks is rather speculative. IR spectra of a 320 μm thick corundum from a South African eclogite assemblage showed no indication for the presence of OH (Rossman and Smyth 1990).

Natural ruby and sapphire samples from crustal origin showed extremely weak absorption bands at 3310, 3230, and 3185 cm^{-1} (Beran 1991). Smith et al. (1995) confirmed OH bands also in sapphires from Southern Vietnam. In a comprehensive IR spectroscopic study of about 150 corundum samples from worldwide localities, Beran and Rossman (2006) established the presence of OH defects in corundum of crustal occurrences, however at concentration levels around only 0.5 wt ppm H_2O or even lower.

On the other hand, knowledge of possible OH defect incorporation mechanisms in this hexagonally close-packed mineral structure has a definite geophysical interest due to its close relation to $MgSiO_3$ akimotoite in the high-PT regions of the Earth's interior. Therefore, a number of synthetic samples have been studied in the past.

OH groups in hydrothermally grown corundum were originally recognized by Belt (1967). A polarized IR spectroscopic study of a suite of Verneuil-grown corundum crystals (Beran 1991) revealed that variously colored samples show a distinct variability in the region of the OH fundamental vibration. Narrow strongly polarized OH bands with varying intensities are centered at 3310, 3230, and 3185 cm^{-1} (see above). Additional weak bands at 3290 cm^{-1} occur in (V Cr Fe Ti)-doped "alexandrite" sapphires, weak bands at 3280 and 3160 cm^{-1} appear in colorless corundum. Due to the strong polarization with maximum absorption perpendicular to the c axis and the deduced orientation of the OH dipoles perpendicular to c, Beran (1991) proposed a model where, under the assumption of vacant Al sites, OH defects are coordinated by two Al atoms, forming groups of face-sharing $[Al_2(OH)O_8]$ double octahedra. According to Moon and Phillips (1991) the OH defects appear to be correlated to vacant Al sites as well as to the presence of Ti^{4+}. In addition, two types of OH absorption bands were reported for hydrothermally treated synthetic sapphires by Kronenberg et al. (2000). The first type of bands observed at 3308, 3293, 3278, 3231, 3208, 3183, and 3163 cm^{-1} is characterized by narrow bands and strong pleochroism, the second type consists of a broad isotropic band centered at 3400 cm^{-1}, resembling closely the OH bands of hydrothermally grown quartz crystals.

Polarized IR spectra of synthetic high-P $MgSiO_3$ akimotoite (Bolfan-Casanova et al. 2002), consist of five pleochroic OH absorption bands—three sharp strong bands at 3390, 3320, and 3300 cm^{-1} and two weak bands at 3260 and 3050 cm^{-1}. Based on Paterson's (1982) calibration the H_2O content was calculated to 350 wt ppm. The bands at 3320 and 3300 cm^{-1} are strongly polarized perpendicular to the c axis. Similar to corundum, under the assumption of Mg vacancies, the pleochroic behavior is consistent with OH groups oriented nearly parallel to the plane of the shared face between two SiO_6 octahedra. The two OH bands of corundum (at 3310 and 3230 cm^{-1}) with the same pleochroic behavior occur at lower frequencies compared to those of $MgSiO_3$ akimotoite. The band at 3390 cm^{-1} has maximum intensity

parallel to the *c* axis and is therefore consistent with OH groups pointing into a tetrahedral void of the close-packed oxygen sublattice. This band, however, has no analogue in the IR spectrum of corundum.

ACKNOWLEDGMENTS

REFERENCES

Aines RD, Rossman GR (1984) The high temperature behavior of water and carbon dioxide in cordierite and beryl. Am Mineral 69:319-327

Aines RD, Rossman GR (1985) The high temperature behavior of trace hydrous components in silicate minerals. Am Mineral 70:1169-1179

Andrut M, Wildner M, Beran A (2002) The crystal chemistry of birefringent natural uvarovites. Part IV. OH defect incorporation mechanisms in non-cubic garnets derived from polarized IR spectroscopy. Eur J Mineral 14:1019-1026

Andrut M, Brandstätter F, Beran A (2003) Trage hydrogen zoning in diopside. Mineral Petrol 78:231-241

Andrut M, Wildner M, Rudowicz CZ (2004) Optical absorption spectroscopy in geosciences. Part II: Quantitative aspects of crystal fields. *In:* Spectroscopic Methods in Mineralogy. Beran A, Libowitzky E (eds) EMU Notes in Mineralogy, vol 6. Eötvös University Press, p 145-188

Asimov PD, Stein LC, Mosenfelder JL, Rossman GR (2006) Quantitative polarized infrared analysis of trace OH in populations of randomly oriented mineral grains. Am Mineral 91:278-284

Armbruster T, Kohler T, Libowitzky E, Friedrich A, Miletich R, Kunz M, Medenbach O, Gutzmer J (2001) Structure, compressibility, hydrogen bonding, and dehydration of the tetragonal Mn^{3+} hydrogarnet, henritermierite. Am Mineral 86:147-158

Aurisicchio C, Grubessi O, Zecchini P (1994) Infrared spectroscopy and crystal chemistry of the beryl group. Can Mineral 32:55-68

Baumer A, Ganteaume M, Klee WE (1985) Determination of OH ions in hydroxyfluorapatites by infrared spectroscopy. Bull Minéral 108:145-152

Bellamy LJ, Owen AJ (1969) A simple relationship between the infrared stretching frequencies and the hydrogen bond distances in crystals. Spectrochim Acta A25:329-333

Bellatreccia F, Della Ventura G, Ottolini L, Libowitzky E, Beran A (2005) The quantitative analysis of OH in vesuvianite: a polarized FTIR and SIMS study. Phys Chem Minerals 32:65-76

Belokoneva EL, Smirnitskaya YuYa, Tsirel'son VG (1993) Electron density distribution in topaz $Al_2(SiO_4)(F,OH)_2$ as a result of accurate X-ray diffraction study. Zhurnal Neorganicheskoi Khimii 38:1346-1350

Belt FR (1967) Hydrothermal ruby: Infrared spectra and X-ray topography. J Appl Phys 38:2688-2689

Beny JM, Piriou B (1987) Vibrational spectra of single-crystal topaz. Phys Chem Minerals 15:148-154

Beran A (1976) Messung des Ultrarot-Pleochroismus von Mineralen. XIV. Der Pleochroismus der OH-Streckfrequenz in Diopsid. Tschermaks Min Petr Mitt 23:79-85

Beran A (1991) Trace hydrogen in Verneuil-grown corundum and its colour varieties - an IR spectroscopic study. Eur J Mineral 3:971-975

Beran A (1999) Contribution of IR spectroscopy to the problem of water in the Earth's mantle. *In:* Microscopic Properties and Processes in Minerals. Wright K, Catlow R (eds) NATO Science Series. Kluwer Acad. Publishers, p 523-538

Beran A (2002) Infrared spectroscopy of micas. Rev Mineral Geochem 46:351-369

Beran A, Libowitzky E (2006) Water in natural mantle minerals II: olivine, garnet and accessory minerals. Rev Mineral Geochem 62:169-191

Beran A, Rossman GR (2006) OH in naturally occurring corundum. Eur J Mineral 18, in press

Beran A, Langer K, Andrut M (1993) Single crystal infrared spectra in the range of OH fundamentals of paragenetic garnet, omphacite and kyanite in an eklogitic mantle xenolith. Mineral Petrol 48:257-268

Beran A, Libowitzky E, Armbruster T (1996) A single-crystal infrared spectroscopic and X-ray diffraction study of untwinned San Benito perovskite containing OH groups. Can Mineral 34:803-809

Beran A, Giester G, Libowitzky E (1997) The hydrogen bond system in natrochalcite-type compounds - An FTIR spectroscopic study of the $H_3O_2^-$ unit. Mineral Petrol 61:223-235

Bolfan-Casanova N (2005) Water in the Earth's mantle. Mineral Mag 69:229-257

Bolfan-Casanova N, Keppler H, Rubie DC (2000) Water partitioning between nominally anhydrous minerals in the MgO-SiO$_2$-H$_2$O system up to 24 GPa: implications for the distribution of water in the Earth's mantle. Earth Planet Sci Lett 182:209-221

Bolfan-Casanova N, Keppler H, Rubie DC (2002) Hydroxyl in MgSiO$_3$ akimotoite: A polarized and high-pressure IR study. Am Mineral 87:603-608

Blanchard M, Wright K, Gale JD (2005) A computer simulation study of OH defects in Mg$_2$SiO$_4$ and Mg$_2$GeO$_4$ spinels. Phys Chem Minerals 32:585-593

Bradbury SE, Williams Q (2003) Contrasting bonding behavior of two hydroxyl-bearing metamorphic minerals under pressure: Clinozoisite and topaz. Am Mineral 88:1460-1470

Braithwaite JS, Wright K, Catlow CRA (2003) A theoretical study of the energetics and IR frequencies of hydroxyl defects in forsterite. J Geophys Res 108(B6):2284

Brigatti MF, Davoli P (1990) Crystal structure refinement of 1M plutonic biotites. Am Mineral 75:305-313

Brown ID (1981) The bond-valence method: An empirical approach to chemical structure and bonding. *In:* Structure and Bonding in Crystals, vol II. O'Keeffe M, Navrotsky A (eds), Academic Press, p 1-30

Burns RG, Strens RGJ (1966) Infrared study of the hydroxyl bands in clinoamphiboles. Science 153:890-892

Buse K, Breer S, Peithmann K, Kapphan S, Gao M, Krätzig E (1997) Origin of thermal fixing in photorefractive lithium niobate crystals. Phys Rev B56:1225-1235

Caruba R, Baumer A, Ganteaume M, Iacconi P (1985) An experimental study of hydroxyl groups and water in synthetic and natural zircons: a model of the metamict state. Am Mineral 70:1224-1231

Dixon JE, Leist L, Langmuir C, Schilling J-G (2002) Recycled dehydrated lithosphere observed in plume-influenced mid-ocean-ridge basalt. Nature 420:385-389

Dobson DP, Meredith PG, Boon SA (2002) Simulation of subduction zone seismicity by dehydration of serpentine. Science 298:1407-1410

Dumas P, Tobin MJ (2003) A bright source for infrared microspectroscopy: synchrotron radiation. Spectr Eur 15/6:17-23

Emsley J, Jones D, Lucas J (1981) Detecting and measuring strong hydrogen bonds: recent developments. Rev Inorg Chem 3:105-140

Fadini A, Schnepel F-M (1989) Vibrational spectroscopy. Ellis Horwood Limited

Gatta GD, Nestola F, Bromiley GD, Mattauch S (2006) The real topological configuration of the extra-framework content in alkali-poor beryl: A multi-methodological study. Am Mineral 91:29-34

Geiger, CA (2004) An introduction to spectroscopic methods in the mineral sciences and geochemistry. *In:* Spectroscopic Methods in Mineralogy. Beran A, Libowitzky E (eds) EMU Notes in Mineralogy, vol 6. Eötvös University Press, p 1-42

Geiger CA, Stahl A, Rossman GR (2000) Single-crystal IR- and UV/VIS- spectroscopic measurements on transition-metal-bearing pyrope: the incorporation of hydroxide in garnet. Eur J Mineral 12:259-271

Gibbs GV, Rosso KM, Cox DF, Boisen Jr MB (2003) A physical basis for Pauling's definition of bond strength. Phys Chem Minerals 30:317-320

Griffiths PR, de Haseth JA (1986) Fourier Transform Infrared Spectrometry (Chem Anal 83). John Wiley & Sons

Griggs D (1967) Hydrolytic weakening of quartz and other silicates. Geophys J R Astr Soc, 14:19-31

Groat LA, Hawthorne FC, Ercit TS (1992) The chemistry of vesuvianite. Can Mineral 30:19-48

Gebert W, Zemann J (1965) Messung des Ultrarot-Pleochroismus von Mineralen. III. Der Pleochroismus der OH-Streckfrequenz in Topas. N Jb Miner Mh 1965:380-384

Hall D, Wood MK (1985): A molecular-packing analysis of the crystal structures of ice. Acta Cryst B41:169-172

Hammer VMF, Libowitzky E, Rossman GR (1998) Single-crystal IR spectroscopy of very strong hydrogen bonds in pectolite, NaCa$_2$[Si$_3$O$_8$(OH)], and serandite, NaMn$_2$[Si$_3$O$_8$(OH)]. Am Mineral 83:569-576

Hirth G, Kohlstedt DL (1996) Water in the oceanic upper mantle: Implications for rheology, melt extraction and the evolution of the lithosphere. Earth Planet Sci Lett 144:93-108

Hu Meisheng, Wenk H-R, Sinitsyna D (1992) Microstructures in natural perovskites. Am Mineral 77:359-373

Ingrin J, Blanchard M (2006) Diffusion of hydrogen in minerals. Rev Mineral Geochem 62:291-320

Ingrin J, Latrous K, Doukhan J-C, Doukhan N (1989) Water in diopside: an electron microscopy and infrared spectroscopy study. Eur J Mineral 1:327-431

Jacobsen SD (2006) Effect of water on the equation of state of nominally anhydrous minerals. Rev Mineral Geochem 62:321-342

Jacobsen SD, van der Lee S (Eds) (2006) Earth's Deep Water Cycle. Am Geophys Union Monogr Ser, in press

Jacobsen SD, Demouchy S, Frost DJ, Boffa Ballaran T, Kung J (2005) A systematic study of OH in hydrous wadsleyite from polarized FTIR spectroscopy and single-crystal X-ray diffraction: Oxygen sites for hydrogen storage in Earth's interior. Am Mineral 90:61-70

Jung H, Green HW (2004) Experimental faulting of serpentinite during dehydration: Implications for earthquakes, seismic low-velocity zones, and anomalous hypocenter distributions in subduction zones. Int Geol Rev 46:1089-1102

Karato S (1990) The role of hydrogen in the electrical conductivity of the upper mantle. Nature 347:272-273

Khisina NR, Wirth R, Andrut M, Ukhanov AV (2001) Extrinsic and intrinsic mode of hydrogen occurrence in natural olivines: FTIR and TEM investigation. Phys Chem Minerals 28:291-301

Khomenko VM, Langer K, Beran A, Koch-Müller M, Fehr T (1994): Titanium substitution and OH-bearing defects in hydrothermally grown pyrope crystals. Phys Chem Minerals 20:483-488

Kleppe AK, Jephcoat AP, Welch MD (2003) The effect of pressure upon hydrogen bonding in chlorite: A Raman spectroscopic study of clinochlore to 26.5 GPa. Am Mineral 88:567-573

Koch-Müller M, Abs-Wurmbach I, Rhede D, Kahlenberg V, Matsyuk, S (2005) Hydration and dehydration of omphacite. Berichte der Deutschen Mineralogischen Ges, Beih z Eur J Mineral 17, No 1:69

Kohlstedt DL, Mackwell SJ (1998) Diffusion of hydrogen and intrinsic point defects in olivine. Z Phys Chem 207:147-162

Kolesov AB, Geiger CA (2000a) A single-crystal Raman study of the orientation and vibrational states of molecular water in beryl. Phys Chem Minerals 27:557-564

Kolesov AB, Geiger CA (2000b) Cordierite II: The role of CO_2 and H_2O. Am Mineral 85:1265-1274

Kronenberg AK, Castaing J, Mitchell TE, Kirby SH (2000) Hydrogen in α-Al_2O_3 and water weakening of sapphire and alumina ceramics between 600 and 1000 °C – I. Infrared characterization of defects. Acta Mater 48:1481-1494

Kurka A (2002) IR-spektroskopische Untersuchungen im OH-Streckschwingungsbereich von Vesuvian und Gossular. MSc thesis, University of Vienna, Austria

Lager GA, Armbruster T, Faber F (1987) Neutron and X-ray diffraction study of hydrogarnet, $Ca_3Al_2(O_4H_4)_3$. Am Mineral 72:756-765

Lager GA, Qianyen X, Ross FK, Rossman GR, Armbruster T, Rotella FJ, Schultz AJ (1999) Hydrogen-atom positions in *P4/nnc* vesuvianite. Can Mineral 37:763-768

Libowitzky E (1999) Correlation of O-H stretching frequencies and O-H···O hydrogen bond lengths in minerals. Mh Chemie 130:1047-1059

Libowitzky E, Beran A (1995) OH-defects in forsterite. Phys Chem Minerals 22:387-392

Libowitzky E, Beran A (2004) IR spectroscopic characterisation of hydrous species in minerals. *In:* Spectroscopic methods in mineralogy. Beran A, Libowitzky E (eds) EMU Notes in Mineralogy, Vol 6. Eötvös University Press, p 227-279

Libowitzky E, Giester G (2003) Washing soda (natron), $Na_2CO_3 \cdot 10H_2O$, revised: Crystal structures at low and ambient temperatures. Mineral Petrol 77:177-195

Libowitzky E, Rossman GR (1996) Principles of quantitative absorbance measurements in anisotropic crystals. Phys Chem Minerals 23:319-327

Libowitzky E, Rossman GR (1997) An IR absorption calibration for water in minerals. Am Mineral 82:1111-1115

Mackwell SJ, Kohlstedt DL, Paterson MS (1985) The role of water in the deformation of olivine single crystals. J Geophys Res 90B:11319-11333

Meade C, Reffner JA, Ito E (1994) Synchrotron infrared absorbance measurements of hydrogen in $MgSiO_3$ perovskite. Science 264:1558-1560

van der Meijde M, Marone F, Giardini D, van der Lee S (2003) Seismic evidence for water deep in Earth's upper mantle. Science 300:1556-1558

Mierdel K, Keppler H (2004) The temperature dependence of water solubility in enstatite. Contr Mineral Petrol 148:305-311

Mikenda W (1986) Stretching frequency versus bond distance correlation of O-D(H)···Y (Y = N, O, S, Se, Cl, Br, I) hydrogen bonds in solid hydrates. J Mol Struct 147:1-15

Moon AR, Phillips MR (1991) Defect clustering in H,Ti:α-Al_2O_3. J Phys Chem Solids 52:1087-1099

Nagai T, Hattori T, Yamanaka T (2000) Compression mechanism of brucite: An investigation by structural refinement under pressure. Am Mineral 85:760-764

Nakamoto K (1977) Infrared and Raman spectra of inorganic and coordination compounds. Wiley, New York

Nakamoto K, Margoshes M, Rundle RE (1955) Stretching frequencies as a function of distances in hydrogen bonds. J Am Chem Soc 77:6480-6486

Novak A (1974) Hydrogen bonding in solids: Correlation of spectroscopic and crystallographic data. Struct Bond 18:177-216

Ohtani E (2005) Water in the mantle. Elements 1:25-30

Parise JB, Cuff C, Moore FH (1980) A neutron diffraction study of topaz: evidence for lower symmetry. Min Mag 43:943-944

Paterson MS (1982) The determination of hydroxyl by infrared absorption in quartz, silicate glasses and similar materials. Bull Minéral 105:20-29

Pauling L (1960) The Nature of the Chemical Bond. Cornell Univ. Press

Ribbe PH, Rosenberg PE (1971) Optical and X-ray determinative methods for fluorine in topaz. Am Mineral 56:1812-1821

Ross NL, Gibbs GV, Rosso KM (2003) Potential docking sites and positions of hydrogen in high-pressure silicates. Am Mineral 88:1452-1459

Rossman GR (1988) Vibrational spectroscopy of hydrous components. Rev Mineral 18:193-206

Rossman GR (2006) Analytical methods for measuring water in nominally anhydrous minerals. Rev Mineral Geochem 62:1-28

Rossman GR, Aines RD (1991) The hydrous components in garnets: Grossular-hydrogrossular. Am Mineral 76: 1153-1164

Rossman GR, Smyth JR (1990) Hydroxyl contents of accessory minerals in mantle eclogites and related rocks. Am Mineral 75: 775-780

Rothbauer R (1971) Untersuchung eines $2M_1$-Muskovits mit Neutronenstrahlen. N Jb Mineral Mh 1971:143-154

Rowbotham G, Farmer VC (1973) The effect of "A" site occupancy upon hydroxyl stretching frequency in clinoamphiboles. Contrib Mineral Petrol 38:147-149

Ryskin YI (1974) The vibrations of protons in minerals: hydroxyl, water and ammonium. *In:* The Infrared Spectra of Minerals. Farmer VC (ed) Mineralogical Society, p 137 -181

Sacerdoti M, Passaglia E (1985) The crystal structure of katoite and implications within the hydrogrossular group of minerals. Bull Minéral 108:1-8

Schiffer J, Intenzo M, Hayward P, Calabrese C (1976) The FS correlation and a systematic analysis of the stretching absorptions of water in the condensed state. J Chem Phys 64:3014-3020

Serratosa JM, Bradley WF (1958) Determination of the orientation of OH bond axes in layer silicates by infrared absorption. J Phys Chem 62:1164-1167

Skogby H (2006) Water in natural mantle minerals I: pyroxenes. Rev Mineral Geochem 62:155-167

Skogby H, Rossman GR (1989) OH⁻ in pyroxene: An experimental study of incorporation mechanisms and stability. Am Mineral 74:1059-1069

Skogby H, Bell DR, Rossman GR (1990) Hydroxide in pyroxene: Variations in the natural environment. Am Mineral 75:764-774

Smith CP, Kammerling RC, Keller AS, Peretti A, Scarratt KV, Khoa ND, Repetto S (1995) Sapphires from southern Vietnam. Gems Gemology 31:168-186

Smyth JR (1987) β-Mg_2SiO_4: A potential host for water in the mantle? Am Mineral 72:1051-1055

Smyth JR, Frost DJ (2002) The effect of water on the 410-km discontinuity: An experimental study. Geophys Res Lett 29:10.1029/2001GL014418

Smyth JR, Bell DR, Rossman GR (1991) Incorporation of hydroxyl in upper-mantle clinopyroxenes. Nature 351:732-735

Smyth JR, Holl CM, Frost DJ, Jacobsen SD, Langenhorst F, McCammon CA (2003) Structural systematics of hydrous ringwoodite and water in Earth's interior. Am Mineral 88:1402-1407

Strens RGJ (1974) The common chain, ribbon, and ring silicates. *In:* The Infrared Spectra of Minerals. Farmer VC (ed) Mineralogical Society, p 305-330

Szalay V, Kovács L, Wöhlecke M, Libowitzky E (2002) Stretching potential and equilibrium length of the OH bond in solids. Chem Phys Lett 354:56-61

Thompson AB (1992) Water in the Earth's upper mantle. Nature 358:295-302

Tillmanns E, Zemann J (1965) Messung des Ultrarot-Pleochroismus von Mineralen. I. Der Pleochroismus der OH-Streckfrequenz in Azurit. N Jb Miner Mh 1965:228-231

Tsuboi M (1950) On the position of the hydrogen atoms in the crystal structure of muscovite, as revealed by the infra-red absorption study. Bull Chem Soc Japan 23:83-88

Urusov VS (1992) A geometric model of deviations from Vegard's rule. J Solid State Chem 98:223-236

Wieczorek A, Libowitzky E, Beran A (2004) A model for the OH defect incorporation in kyanite based on polarised IR spectroscopic investigations. Schweiz Min Petr Mitt 84:333-343

Wilkins RWT, Sabine W (1973) Water content of some nominally anhydrous silicates. Am Mineral 58:508-516

Winkler B (1996) The dynamics of H_2O in minerals. Phys Chem Minerals 23:310-318

Wright K (2006) Atomistic models of OH defects in nominally anhydrous minerals. Rev Mineral Geochem 62:67-83

Wunder B, Andrut M, Wirth R (1999) High-pressure synthesis and properties of OH-rich topaz. Eur J Mineral 11:803-813

Zemann J, Zobetz, E, Heger G, Völlenkle H (1979) Strukturbestimmung eines OH-reichen Topases. Anz Österr Akad Wiss, Math-Naturwiss Kl 116:145-147